On postglacial sea level—III. Incorporating sediment redistribution

Permanent link

http://nrs.harvard.edu/urn-3:HUL.InstRepos:41401411

Share Your Story

Accessibility

On postglacial sea level—III. Incorporating sediment redistribution

A. V. Dalca,[1] K. L. Ferrier,[2] J. X. Mitrovica,[2] J. T. Perron,[3] G. A. Milne[4] and J. R. Creveling[5]

[1]*Computer Science and Artificial Intelligence Lab, MIT, Cambridge, MA* 02139, *USA. E-mail: adalca@mit.edu*
[2]*Department of Earth and Planetary Sciences, Harvard University, Cambridge, MA* 02138, *USA*
[3]*Department of Earth, Atmospheric and Planetary Sciences, MIT, Cambridge, MA* 02139, *USA*
[4]*Department of Earth Sciences, University of Ottawa, Ottawa, ON K1N 6N5, Canada*
[5]*Division of Geological and Planetary Sciences, California Institute of Technology, Pasadena, CA* 91125, *USA*

SUMMARY
We derive a generalized theory for gravitationally self-consistent, static sea level variations on earth models of arbitrary complexity that takes into account the redistribution of sediments. The theory is an extension of previous work that incorporated, into the governing equations, shoreline migration due to local sea level variations and changes in the geometry of grounded, marine-based ice. In addition, we use viscoelastic Love number theory to present a version of the new theory valid for spherically symmetric earth models. The Love number theory accounts for the gravitational, deformational and rotational effects of the sediment redistribution. As a first, illustrative application of the new theory, we compute the perturbation in sea level driven by an idealized pulse of sediment transport into the Gulf of Mexico. We demonstrate that incorporating a gravitationally self-consistent water load in this case significantly improves the accuracy of sea level predictions relative to previous simplified treatments of the sediment redistribution.

Key words: Sea level change; Geomorphology; Sedimentary basin processes; Tectonics and landscape evolution.

1 INTRODUCTION

Numerical predictions of postglacial sea level change have been instrumental in advancing our understanding of Earth's internal structure, ice age and modern climate, Quaternary geomorphology and human migration. All modern predictions of sea level changes in response to the melting of Late Pleistocene ice complexes may be traced to the seminal work of Farrell & Clark (1976, henceforth FC76). FC76 derived a so-called 'sea level equation' which governed the gravitationally self-consistent redistribution of meltwater on a viscoelastic, non-rotating earth model in the case where shorelines remained fixed to their present-day location. In practical terms, this treatment of shorelines is equivalent to assuming that shorelines are characterized by steep vertical cliffs, so that local changes in sea level do not produce transgressions or regressions, and that there is no change in the geometry of grounded marine-based ice.

The FC76 derivations are based on an equilibrium (i.e. static) sea level theory in which the distribution of meltwater at any time is determined by the contemporaneous gravitational and solid Earth deformational fields. (This is distinct from non-equilibrium sea level theories applied to, for instance, short-period tides, in which one cannot neglect inertia in the oceans and forces such as bottom friction.) However, even with this assumption, which is accurate on glacial isostatic adjustment (GIA) timescales, the physics governing sea level change remains complex. In particular, the redistribution of meltwater perturbs the gravitational field, both through its direct attraction and via solid Earth deformation, and this redistribution is, in turn, governed by these perturbations. This circularity is reflected in the non-linear, integral nature of the sea level equation derived by FC76.

It is useful to consider the FC76 theory as comprising two independent parts. The first involves a mapping between sea level changes, which are defined globally, and ocean load changes, which are limited to the geometry of the ocean basins. Under the assumption of fixed shorelines, this projection is trivial; one simply multiplies the sea level change by the so-called ocean function, which is defined to be unity over the oceans and zero elsewhere. The second part of the theory describes a methodology for computing perturbations in both the gravitational field of the planet and vertical deformations of the solid surface driven by an arbitrary surface mass load history. For this purpose, FC76 assume a spherically symmetric, self-gravitating, non-rotating, Maxwell viscoelastic earth model and they derive Green's functions using viscoelastic Love number theory (Peltier 1974).

The initial implementation of the FC76 theory (e.g. Peltier & Andrews 1976; Clark *et al.* 1978; Peltier *et al.* 1978; Wu & Peltier 1983; Tushingham & Peltier 1991) was based on a computation of the Green's functions in the space domain using a circular disk load

discretization of the Earth's surface . Fully spectral and pseudospectral solutions of the sea level equation (Mitrovica & Peltier 1991) have since become the standard approach in the GIA community. In these solutions, all calculations are performed in the spectral domain with the exception of the projection of sea level onto the ocean function.

Since the early 1990s, there have been advancements in both aspects of the FC76 sea level theory. First, a number of studies have extended the surface mass loading theory to include rotational effects (e.g. Milne & Mitrovica 1996, 1998) and to consider the response of earth models with 3-D variations in viscoelastic structure (e.g. Martinec 2000; Wu & van der Wal 2003; Zhong *et al.* 2003; Latychev *et al.* 2005). These extensions have been applied in several studies of postglacial sea level changes (Wu & van der Wal 2003; Paulson *et al.* 2005; Kendall *et al.* 2006; Davis *et al.* 2008) . Secondly, a series of independent efforts have treated the case of shoreline migration due to local changes in sea level (Johnston 1993; Peltier 1994; Milne 1998; Milne *et al.* 1999) and/or the growth and ablation of grounded, marine-based ice (Milne 1998; Peltier 1998; Milne *et al.* 1999; see also Lambeck *et al.* 2003). The distinct treatment of shoreline migration among these studies was the source of a debate within the GIA literature that is now resolved (see Mitrovica 2003 for a detailed review). In particular, Mitrovica & Milne (2003) and Kendall *et al.* (2005) developed a generalized, exact treatment of time-dependent shorelines in a revised sea level equation, and they used schematic illustrations and quantitative predictions to assess the relative accuracy of previous formulations.

In this study, our goal is to extend the global sea level theory derived by Mitrovica & Milne (2003) and Kendall *et al.* (2005) to incorporate, in a gravitationally self-consistent fashion, the impact of sediment redistribution into the existing treatment of ice and ocean water redistribution. The effects of a sediment load differ from those of an ice load. In particular, grounded marine-based ice within oceanic regions will displace all of the local ocean (i.e. water and grounded marine ice cannot coexist at a specific location), and thus the existence of such ice acts to redefine the shoreline and ocean geometry. In contrast, sediment packages pushed offshore, for example, are not necessarily thick enough to displace the entire column of ocean water. That is, sediments can coexist with ocean water, and thus sediment redistribution will not necessarily lead to a change in the bounding shoreline geometry.

Our theory will assume that the large-scale redistribution of sediment is known *a priori*, or that it can be parametrized in terms of the space–time geometry of the Late Pleistocene ice history. That is, we treat the transfer of sediment as a known input. We note that there has been an attempt to incorporate such transport into postglacial sea level predictions, at least on a regional scale (Simms *et al.* 2007). However, the study neglected the loading effect of sediment-displaced water. The theory described below is global and it incorporates gravitationally self-consistent ocean loading.

We begin with a derivation of the extended sea level theory. To avoid confusion, we adopt the notation used by Mitrovica & Milne (2003) and Kendall *et al.* (2005). The development begins with a generalized case valid for earth models of arbitrary complexity, and then proceeds to the special case of spherically symmetric models. In each case, we provide details of the associated numerical algorithm, with the spherically symmetric case being based on the same pseudospectral methodology used in previous studies (Mitrovica & Peltier 1991). We then illustrate the new sea level equation with a series of schematic diagrams. We end the paper with a case study that applies the spherically symmetric version of the new the-

ory to consider the time-dependent impact on postglacial sea level histories of a simple pulse of sediment transport into the Gulf of Mexico. We show that significant errors may be introduced in sea level calculations when the effects of sediment redistribution are computed using approximate theories that are not gravitationally self-consistent.

2 A GENERALIZED SEA LEVEL EQUATION

2.1 Derivation of a generalized sea level equation

We begin by defining the height of the solid Earth (i.e. the crustal surface not including sediment and ice cover), the height of the sea-surface equipotential (i.e. absolute sea level) and the thicknesses of sediment and ice. From these fields, we construct an expression for sea level and ocean load changes. Each of the fields has a dependence on space (via colatitude θ and east longitude ψ) and time t. In this section, we adopt a notation that suppresses these explicit dependencies for the sake of simplicity. That is, we write a generic function $\chi(\theta, \psi, t_j)$ more compactly as χ, or χ_j when it is necessary to make the time dependence explicit. Under this notation, let

$R \equiv$ The height of the Earth's bedrock surface;

$G \equiv$ The height of the equipotential that defines the sea surface;

$H \equiv$ Sediment thickness;

$I \equiv$ Thickness of land-based and grounded marine-based ice. (1)

The fields R, H, I and G are shown schematically in Figs 1(b) and (c) for a general configuration of ice, water, sediment and solid Earth given in Fig. 1(a). The height of the solid surface of the planet is given by $R + H + I$, and sea level is defined as the height of the sea-surface equipotential relative to this solid surface datum:

$$SL = G - (R + H + I). \tag{2}$$

Using this definition of sea level, the topography is then simply given by

$$T = (R + H + I) - G$$
$$= -SL. \tag{3}$$

This expression for topography is in accord with the usual field quantity, as specified in data sets such as ETOPO2 (US Dept of Commerce 2001). Fig. 1(d) provides a schematic illustration of sea level, *SL*, and topography, *T*, in the case of the scenario shown in Fig. 1(a).

While sea level is defined globally, the ocean thickness is clearly non-zero only over oceanic regions. Mathematically, this thickness is given by a projection of the sea level onto the oceans

$$S = SL \cdot C, \tag{4}$$

where C is the ocean function (Munk & Macdonald 1960)

$$C = \begin{cases} 1 & \text{if } SL > 0 \\ 0 & \text{if } SL \le 0. \end{cases} \tag{5}$$

Both the ocean thickness S and the ocean function C depend on the sea level *SL*. The relation between *SL*, *C* and *S* is illustrated in Fig. 1(e).
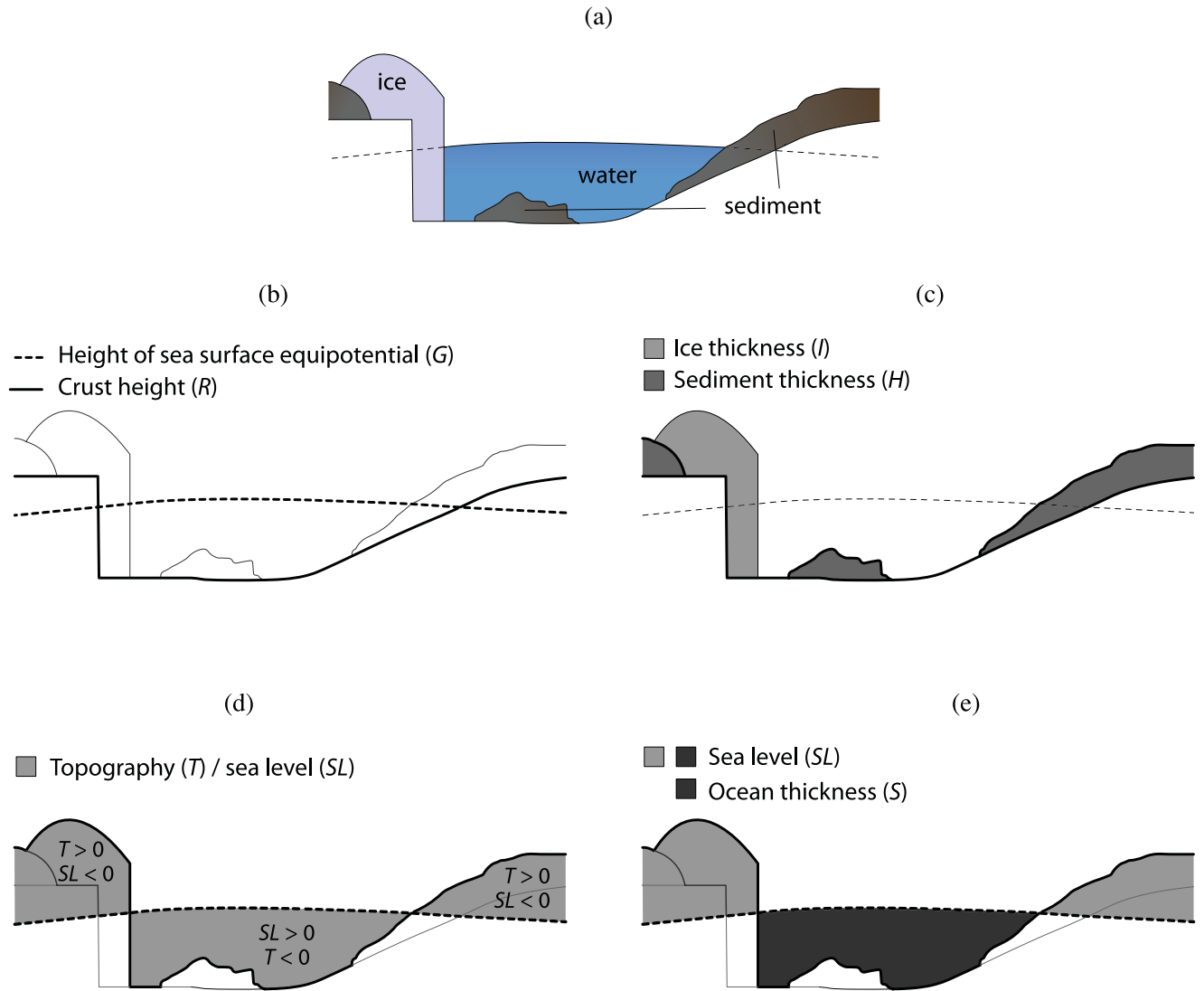
Figure 1. Schematic illustration of the fields adopted within the sea level theory of the text. Panel (a) shows a general configuration of ocean, sediment, ice and the underlying solid crust. Panel (b) shows the same configuration as that in (a), and highlights the heights of the sea-surface equipotential G and Earth's crust R (i.e. solid surface minus sediment and ice). Panel (c) highlights the thicknesses of ice I and sediment H; panel (d) identifies the sea level and topography fields SL and T defined by eqs (2) and (3), respectively; and panel (e) shows the same sea level field SL, which is defined everywhere, and the ocean thickness field S, which is non-zero only where there is sea water (i.e. where $SL > 0$; eqs 4 and 5).

Next, we define the surface mass load, which is comprised of the oceans, ice and sediments

$$L = \rho_{\mathrm{w}} S + \rho_{\mathrm{I}} I + \rho_{\mathrm{H}} H, \tag{6}$$

where ρ_{w}, ρ_{I} and ρ_{H} are the densities of water, ice and sediment, respectively.

We are concerned with predicted perturbations in the quantities SL, T, S, G and R associated with isostatic adjustments driven by surface mass (ice, water and sediment) loading. Henceforth, we retain the usual term 'glacial isostatic adjustment' for this more general scenario. In this regard, we distinguish between variations from the onset of loading and between two successive time steps in the numerical evolution of the system. Let us consider some general time-dependent field χ_j. A perturbation in this field from the onset of loading, at time t_0, is given by

$$\Delta \chi_j = \chi_j - \chi_0$$

$$\Rightarrow \chi_j = \chi_0 + \Delta \chi_j. \tag{7}$$

If, instead, we consider a variation over successive time steps, we write

$$\delta \chi_j = \chi_j - \chi_{j-1}$$

$$= (\chi_j - \chi_0) - (\chi_{j-1} - \chi_0)$$

$$= \Delta \chi_j - \Delta \chi_{j-1}. \tag{8}$$

From eqs (7) and (8), it is apparent that the total variation since the onset of loading can be written in terms of the variations between successive time steps.

$$\Delta \chi_j = \sum_{n=1}^{j} \delta \chi_n. \tag{9}$$

The expressions (7) and (8) may be applied to any of the fields R, H, I, G, SL, T, S and L. For example, from (2), (7) and (8), we have

$$\Delta SL_j = SL_j - SL_0 = \Delta G_j - (\Delta R_j + \Delta H_j + \Delta I_j) \tag{10}$$

and

$$\delta SL_j = SL_j - SL_{j-1} = \delta G_j - (\delta R_j + \delta H_j + \delta I_j). \qquad (11)$$

Since the ocean thickness involves the projection of sea level onto the ocean function, a variation in this thickness cannot be written as a simple combination of the variation in the fields G, R, I, etc. Instead, we begin by writing

$$\Delta S_j = S_j - S_0$$
$$= SL_j C_j - SL_0 C_0. \qquad (12)$$

Then, applying the general eq. (7) to the sea level change (i.e. setting $\chi = SL$ in this equation) and using this in eq. (12) yields

$$\Delta S_j = \Delta SL_j C_j + SL_0[C_j - C_0], \qquad (13)$$

$$\boxed{\Delta S_j = \Delta SL_j C_j - T_0[C_j - C_0].} \qquad (14)$$

Similarly, from eq. (8)

$$\delta S_j = \Delta S_j - \Delta S_{j-1}$$
$$= SL_j C_j - SL_{j-1} C_{j-1}. \qquad (15)$$

Using the expression for ΔS_j in eq. (15) gives

$$\boxed{\delta S_j = -\Delta S_{j-1} + \Delta SL_j C_j - T_0[C_j - C_0].} \qquad (16)$$

In eqs (14) and (16), we have used the simple relationship between sea level and topography in eq. (3).

Eqs (14) or (16), combined with eqs (3), (5) and (10), represent the generalized form of the sea level equation valid for a scenario that includes redistribution of ice, meltwater and sediments. In the context of the discussion in the Introduction, these equations provide an exact mapping between global postglacial sea level variations, ΔSL, and the variation in the ocean thickness. They thus represent an extension to the classic, fixed-shoreline treatment of FC76, as well as the time evolving shoreline theory (in the absence of sediment redistribution) of Mitrovica & Milne (2003) and Kendall *et al.* (2005), that is rooted in the definition of SL given by eq. (2).

Eq. (14) has a clear physical interpretation. The first term on the right-hand side represents a projection of the total sea level variation at time t_j onto the ocean function at this same time. Thus, the total variation in the ocean thickness at t_j, ΔS_j, is equal to a combination of this term, which is the only term appearing in the fixed-shoreline FC76 theory, and a correction term that accounts for any shoreline evolution. The latter term is a projection of the original sea level field, SL_0 (or T_0), onto a function which is only non-zero within the zone of shoreline migration from time t_0 to t_j (i.e. $C_j - C_0$).

It will be instructive to highlight the physical meaning of eq. (15) using a simple set of schematics. To begin, Fig. 2 shows a redistribution of sediment, ice and water and a deformation of the solid Earth from the state shown in Fig. 1(a) (which we associate with $t = t_{j-1}$) to a new state at $t = t_j$ (Fig. 2b). Below each frame we specify the value of the ocean function (zero or one) and the ocean thickness (zero or sea level SL) in each region of the schematic. The last line below the figure lists δS_j, the difference in ocean thickness between time steps t_j and t_{j-1}. These values of δS_j highlight the interplay between sediment and ice redistribution and the change in the ocean thickness, which represents the change in the ocean load.

In Fig. 3, we confirm the validity of the generalized sea-level eq. (14) using a simple redistribution of sediment and water. The top frame shows the initial condition (i.e. $t = t_0$). Fig. 3(b) shows a snapshot at some time later, $t = t_j$, at which point the sediment on

land in Fig. 3(a) has entered the ocean, forming an island, while the sediment within the ocean in Fig. 3(a) has slumped to fall below the local sea surface. These changes alter the ocean function, as indicated by the summary values for C and S below each frame. In Fig. 3(c), we use the geometries in the first two frames to directly compute the change in the ocean thickness (load), and the results are shown both as a schematic and in a list of values below this schematic. Finally, we provide a table which uses the expressions in the first two frames to implement the generalized sea level eq. (14) governing the ocean thickness change since the onset of the loading (i.e. since $t = t_0$). The equivalence between these expressions and the values generated by direct inspection of Figs 3(a) and (b) (see bottom of Fig. 3b) confirms the accuracy of the sea level eq. (14).

2.2 Some practical considerations

The generalized sea level eqs (14) or (16) involve the expression (10) for the total variation in sea level. Within this latter expression, ΔI and ΔH are *a priori* inputs (i.e. *a priori* models of the ice history and sediment redistribution), whereas the total postglacial variation in the Earth's sea surface and solid surface height, ΔG and ΔR, respectively, must be computed from some independent calculation that accounts for the full time history of surface mass (ice plus sediment plus ocean) loading. In practical applications of the model, conservation of sediment mass provides an additional constraint on the inputs for ΔH and δH: the integrated mass of eroded sediment over the basin of interest should match the integrated mass of deposited sediment over the deposition area. Using eqs (6) and (7), the time history of the net mass loading may be written as the combination

$$\Delta L_j = \rho_{\mathrm{W}} \Delta S_j + \rho_{\mathrm{I}} \Delta I_j + \rho_{\mathrm{H}} \Delta H_j. \qquad (17)$$

The method of computing ΔSL from the history of loading given by eq. (17) will depend on the complexity of the viscoelastic earth model. For spherically symmetric earth models, this second element of any postglacial sea level theory (see Introduction) may be performed using viscoelastic Love number theory (Peltier 1974), as in FC76. For earth models that incorporate 3-D variations in structure, the calculation of ΔSL can make use of any one of a suite of recently developed spectral finite element and finite volume treatments of the surface loading problem (see Introduction for a list of such studies). Note that in either case, the computation of ΔSL accounts for the gravitational, deformational and rotational perturbations driven by the total surface mass load, including the sediment load history, ΔH.

The suite of expressions (5), (10), (14) and (17) illustrates the integral nature of the sea level equation. Specifically, the calculation of the total ocean thickness change, via eq. (14) requires a determination of both the total variation in sea level and the ocean function, with the latter dependent on the total sea level from eq. (5). However, from eqs (10) and (17), the variation in sea level is clearly a function of the surface mass load and, in particular, the ocean thickness. Physically, the change in ocean thickness is governed (via eqs 5, 10 and 14) by perturbations in the gravitational field, solid surface and ocean function, but these perturbations are, in turn, influenced by ocean loading (i.e. ΔS appears in eq. 17). In practice, this circularity is addressed numerically using an iterative scheme applied at each time step in the sea level solution, in which a first guess to the change in the ocean load from the last time step (i.e. δS_j) is successively improved (see Section 2.4, Mitrovica & Peltier 1991; Mitrovica & Milne 2003; Kendall *et al.* 2005). At each time step,
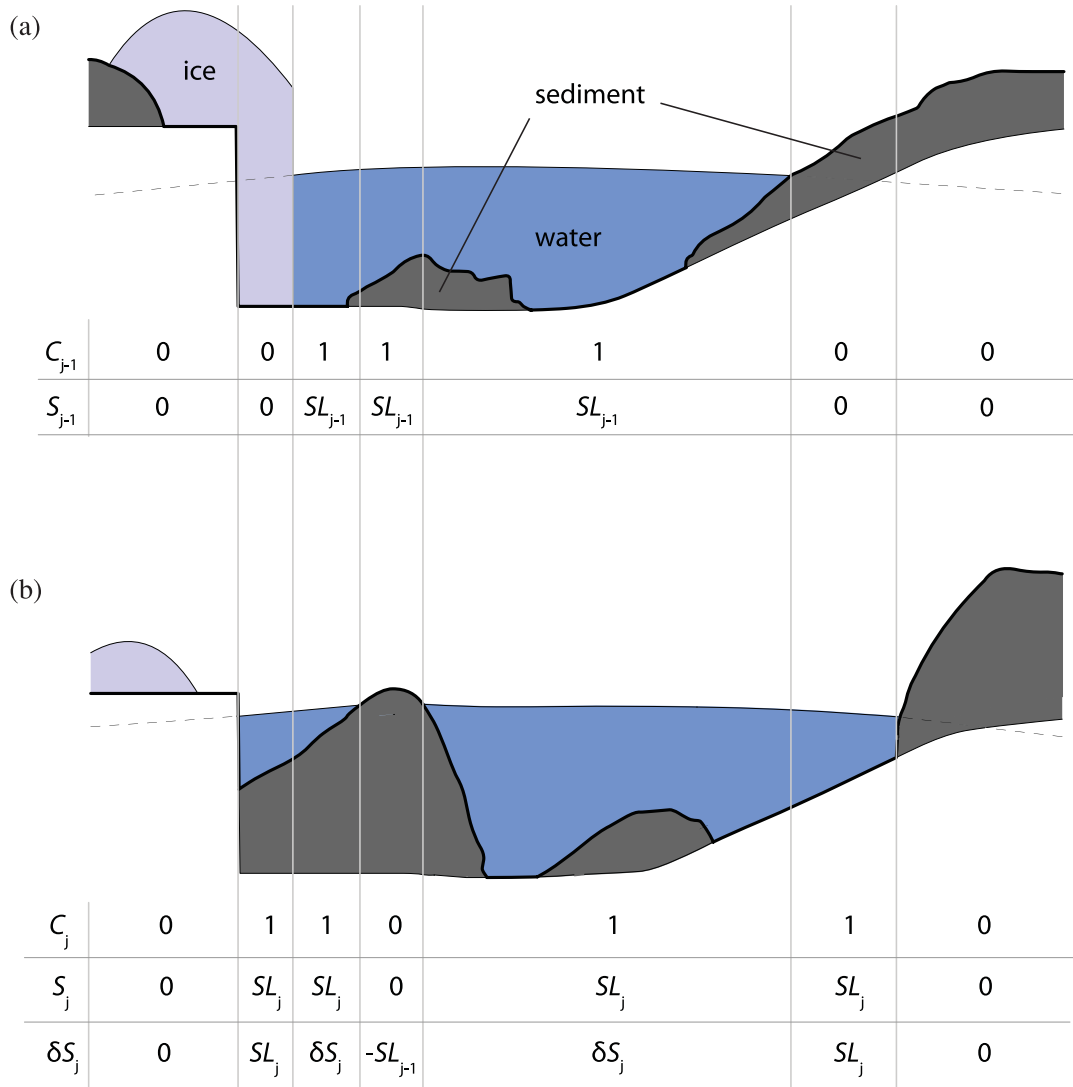
Figure 2. Schematic depicting a redistribution of ice, water and sediment, and deformation of the solid Earth from the situation in Fig. 1(a) (repeated here in the top frame), to a new configuration shown in the bottom frame. The frames represent the system at two successive time steps in the evolution, t_{j-1} and t_j, respectively. We list, beneath each frame, the associated value of the ocean function C and the ocean thickness S (the thickness is expressed as being equal to zero or equal to the sea level, where the lateral variation in the latter is suppressed). The final line below the bottom frame provides, following eq. (15), an expression for the change in the water thickness (or load) between the successive time steps (i.e. $\delta S_j = SL_j C_j - SL_{j-1} C_{j-1}$).

we take the first guess in the iterative scheme to be the eustatic sea level change.

In most practical applications, the appearance of the initial topography in the sea level eqs (14) and (16) introduces a second iteration in the postglacial sea level theory since this topography cannot be known at the outset of Late Pleistocene loading (Peltier 1994; Mitrovica & Milne 2003; Kendall *et al.* 2005). Since eqs (7) and (8) hold for the topography, T, then

$$T_j = T_0 + \Delta T_j \tag{18}$$

and, for the present time $t_j = t_p$,

$$T_0 = T_p - \Delta T_p$$

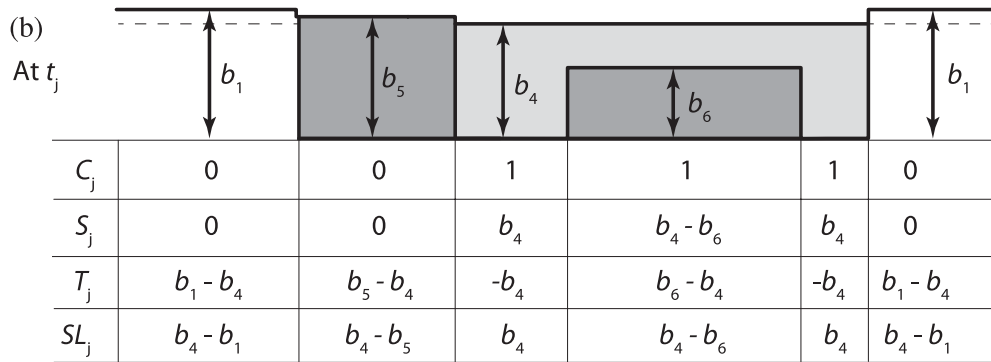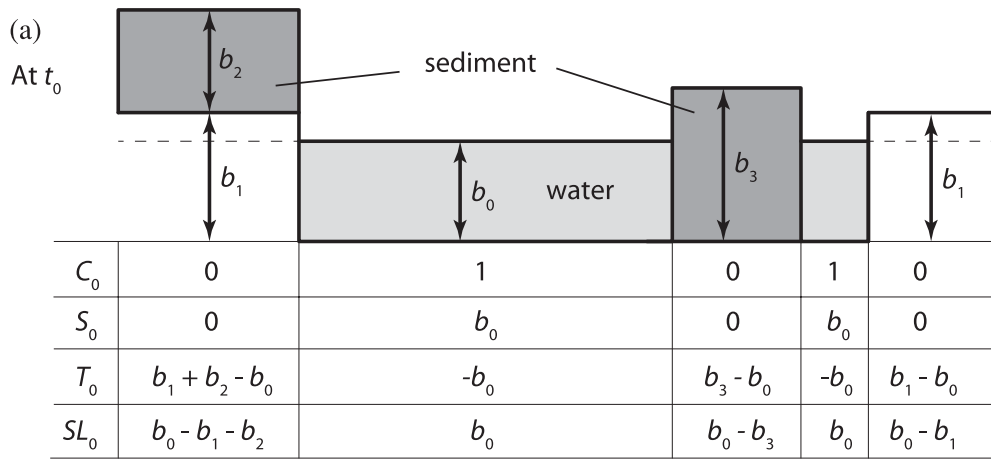$$= T_p + \Delta SL_p. \tag{19}$$

Eq. (19) suggests an algorithm for iteratively improving a first guess to the initial topography. Specifically, the present-day topography, T_p, is known, and a first guess to the initial topography, T_0, is used within the sea level eq. (14) to compute a time history of the total

sea level variation, ΔSL. The present-day value of the latter can then be used in eq. (19) to generate an improved, second iterate value of the initial topography, T_0. This iteration can be repeated until the estimate for T_0 converges within some specified tolerance.

As a final point in this section, we comment on an important check on the ice height, I. The ice height field to be used in eq. (17) refers only to variations in land-based and grounded, marine-based ice. From eq. (2), land-based ice may be defined as being any ice located where $SL + I$ is negative, that is, anywhere in which the topography, when the height of ice is removed, is positive. In the case where the topography after any ice height correction is negative, that is, $SL + I > 0$, ice can only be grounded if its height satisfies the following:

$$I_j > (SL_j + I_j)\frac{\rho_w}{\rho_I} \tag{20}$$

otherwise the ice will be floating. Thus, at any stage of the numerical sea level solution (see below), the *a priori* Late Pleistocene ice history adopted for the calculation will be modified in the following

(a)
At t_0

sediment

b_2 | b_3
b_1 | b_0 water | b_1

C_0	0	1	0	1	0
S_0	0	b_0	0	b_0	0
T_0	$b_1 + b_2 - b_0$	$-b_0$	$b_3 - b_0$	$-b_0$	$b_1 - b_0$
SL_0	$b_0 - b_1 - b_2$	b_0	$b_0 - b_3$	b_0	$b_0 - b_1$

(b)
At t_j

b_1 | b_5 | b_4 | b_6 | b_1

C_j	0	0	1	1	1	0
S_j	0	0	b_4	$b_4 - b_6$	b_4	0
T_j	$b_1 - b_4$	$b_5 - b_4$	$-b_4$	$b_6 - b_4$	$-b_4$	$b_1 - b_4$
SL_j	$b_4 - b_1$	$b_4 - b_5$	b_4	$b_4 - b_6$	b_4	$b_4 - b_1$

The change in ocean thickness ΔS_j can be determined by inspection of (A) and (B). For conciseness, we define

$$\Delta b_a = b_4 - b_0$$
$$\Delta b_b = b_3 - b_0$$
$$\Delta b_c = b_4 - b_6.$$

ΔS_j	0	$-b_0$	Δb_a	$\Delta b_c - b_0$	Δb_c	Δb_a	0

(c) ΔS_j determined with the generalized sea-level equation (equation 14).

$\Delta SL_j C_j$	0	0	Δb_a	$\Delta b_c - b_0$	$\Delta b_c + \Delta b_b$	Δb_a	0
$T_0(C_j - C_0)$	0	b_0	0	0	Δb_b	0	0
ΔS_j	0	$-b_0$	Δb_a	$\Delta b_c - b_0$	Δb_c	Δb_a	0

Figure 3. Schematic demonstrating the validity of the generalized sea level eq. (14) for the simple case of a redistribution of sediment and water from an initial state (t_0; frame a) to a final state (t_j; frame b). Below each frame are listed expressions for the ocean function C and the ocean thickness S in each region. Below frame (a) are also expressions for the initial topography T_0. The change in the ocean thickness ΔS_j is computed directly from these two frames, and the result is shown in frame (c), in which shaded areas represent changes in S between t_0 and t_j. Below frame (c) are quantitative expressions required to calculate the change in water load ΔS_j with the generalized sea level equation $\Delta S_j = \Delta SL_j C_j - T_0(C_j - C_0)$ (eq. 14).

fashion:

$$
I_j = \begin{cases} \text{Ice Height} & SL_j + \text{Ice Height} < 0 \\ \text{Ice Height} & SL_j + \text{Ice Height} > 0 \\ & \text{and Ice Height} > SL_j \frac{\rho_{\mathrm{w}}}{\rho_{\mathrm{I}} - \rho_{\mathrm{w}}} \\ 0 & \text{elsewhere.} \end{cases}
\tag{21}
$$

2.3 Decomposing ΔSL into spatially variable and spatially uniform terms

With no loss of generality, it will be instructive to split the perturbation in the height of the sea-surface equipotential into spatially varying and spatially uniform components.

$$
\Delta G_j = \Delta \mathcal{G}_j + \frac{\Delta \Phi_j}{g}.
\tag{22}
$$

Here, the first term on the right-hand side of the equation is the spatially varying component. The second term on the right-hand side is the spatially uniform shift in the height of the sea-surface equipotential, and g is the surface gravitational acceleration. In this case, the total variation in sea level from the onset of loading may be written as

$$
\Delta SL_j = \Delta \mathcal{SL}_j + \frac{\Delta \Phi_j}{g},
\tag{23}
$$

where from eq. (10),

$$
\Delta \mathcal{SL}_j = \Delta \mathcal{G}_j - (\Delta R_j + \Delta H_j + \Delta I_j).
\tag{24}
$$

Using this expression, the generalized sea level eqs (14) and (16) may be rewritten as

$$
\Delta S_j = \Delta \mathcal{SL}_j C_j + \frac{\Delta \Phi_j}{g} C_j - T_0[C_j - C_0]
\tag{25}
$$

and

$$
\delta S_j = -\Delta S_{j-1} + \Delta \mathcal{SL}_j C_j + \frac{\Delta \Phi_j}{g} C_j - T_0[C_j - C_0].
\tag{26}
$$

An expression for the spatially uniform term $\Delta \Phi_j / g$ may be derived by invoking conservation of mass for the total surface mass load. The change in the ocean height integrated over the surface of the Earth—that is, the change in the volume of the ocean—must be connected to changes in the ice volume by

$$
\iint_\Omega \Delta I_j \, d\Omega = -\frac{\rho_{\mathrm{w}}}{\rho_{\mathrm{I}}} \iint_\Omega \Delta S_j \, d\Omega.
\tag{27}
$$

Integrating (25) over the surface of the Earth, and using eq. (27), yields

$$
\frac{\Delta \Phi_j}{g} = -\frac{1}{\mathcal{A}_j} \frac{\rho_{\mathrm{I}}}{\rho_{\mathrm{w}}} \iint_\Omega \Delta I_j \, d\Omega - \frac{1}{\mathcal{A}_j} \iint_\Omega \Delta \mathcal{SL}_j C_j \, d\Omega
$$
$$
+ \frac{1}{\mathcal{A}_j} \iint_\Omega T_0[C_j - C_0] \, d\Omega,
\tag{28}
$$

where

$$
\mathcal{A}_j \equiv \iint_\Omega C_j \, d\Omega.
\tag{29}
$$

Eqs (3), (5), (24)–(26), (28) and (29) represent the complete system of equations that define the generalized sea level theory.

2.4 Numerical implementation

Following Kendall *et al.* (2005), we briefly review an efficient iterative algorithm for solving the new generalized sea level eq. (25). As described earlier, this algorithm is defined by two nested iterations. The inner iteration, denoted here by the counter i, is applied at each time step in the numerical solution to successively refine an initial guess to the ocean height change, $\delta S_j^{i=1}$, for the time step from t_{j-1} to t_j, until convergence (denoted by $\delta S_j^{i=\infty}$) is obtained. The outer iteration, denoted here by counter k, loops over the full set of glacial cycles to improve a first guess for the initial topography field, $T_0^{k=1}$ until convergence (denoted by $T_0^{k=\infty}$).

Using this scheme, we can rewrite the sea level equation in algorithmic form for each iteration (i, k).

$$
\delta S_j^{i,k} = -\Delta S_{j-1}^{i=\infty,k} + \Delta \mathcal{SL}_j^{i-1,k} C_j^{k-1} + \frac{\Delta \Phi(t_j)^{i-1,k}}{g} C_j^{k-1}
$$
$$
- T_0^{k-1}[C_j^{k-1} - C_0^{k-1}].
\tag{30}
$$

The numerical scheme proceeds as follows. Let us assume that the $k-1$ pass through the full loading history has been completed. Using the suite of sea level solutions computed for this outer iteration, we can update the time-dependent topography. From eqs (18) and (19), we have

$$
T_j^{k-1} = T_p + \Delta SL_p^{i=\infty,k-1} - \Delta SL_j^{i=\infty,k-1},
\tag{31}
$$

and, from eq. (5), we can update the time-varying ocean function using

$$
C_j^{k-1} = \begin{cases} 1 & \text{if } T_j^{k-1} < 0, \\ 0 & \text{if } T_j^{k-1} \geq 0. \end{cases}
\tag{32}
$$

Finally, we also use the updated topography to apply the check for grounded ice and refine the input ice load if necessary.

With the topography and ocean function estimates, we proceed onto a calculation of sea level change for the kth iteration. This calculation is based on eq. (24).

$$
\Delta \mathcal{SL}_j^{i-1,k} = \Delta \mathcal{G}_j^{i-1,k} - \left(\Delta R_j^{i-1,k} + \Delta H_j + \Delta I_j^{k-1} \right).
\tag{33}
$$

The inner iteration begins with a guess to the ocean thickness change $\delta S_j^{i-1,k}$ for $i = 1$. Since the sea-surface equipotential and solid surface displacement increments in eq. (33) depend on the surface mass load, including the ocean thickness components (eq. 17), they are also superscripted with the iteration indices. To complete the terms for the right-hand side of eq. (30), we require an expression for the spatially invariant component of the sea-surface equipotential change. From eq. (28), we obtain

$$
\frac{\Delta \Phi_j^{i-1,k}}{g} =
$$
$$
\frac{-1}{\mathcal{A}_j^{k-1}} \frac{\rho_{\mathrm{I}}}{\rho_{\mathrm{w}}} \iint_\Omega \Delta I_j^{k-1} \, d\Omega - \frac{1}{\mathcal{A}_j^{k-1}} \iint_\Omega \Delta \mathcal{SL}_j^{i-1,k} C_j^{k-1} \, d\Omega
$$
$$
+ \frac{1}{\mathcal{A}_j^{k-1}} \iint_\Omega T_0^{k-1} \left[C_j^{k-1} - C_0^{k-1} \right] d\Omega,
\tag{34}
$$

where

$$
\mathcal{A}_j^{k-1} = \iint_\Omega C_j^{k-1} \, d\Omega.
\tag{35}
$$

With this set of equations we can successively refine the ocean thickness and sea level change via eq. (30) until convergence, and then move to the next time step until we make one more pass through the complete loading history. The entire process is repeated until the outer k iteration converges and a final set of topography and ocean function fields are computed. A detailed discussion of the appropriate first guess within each of the inner and outer iteration schemes is described in Kendall *et al.* (2005).

2.5 A comparison with Mitrovica & Milne (2003)

In addition to the inclusion of sediment redistribution, the generalized sea level theory we have outlined here differs from the approach derived by Mitrovica & Milne (2003) and Kendall *et al.* (2005) in one important regard. In particular, in Mitrovica & Milne (2003) and Kendall *et al.* (2005), the expression for sea level did not include the ice height. To illustrate this difference, let us consider a version of our new theory in which sediments play no role. In this case, we can rewrite eqs (2), (4) and (5) as

$$SL^N = G - (R + I),$$ (36)

$$S^N = SL^N \cdot C^N$$ (37)

and

$$C^N = \begin{cases} 1 & \text{if } SL^N > 0 \\ 0 & \text{if } SL^N \le 0, \end{cases}$$ (38)

where the superscript 'N' denotes this special no sediment case of our new sea level formalism.

In contrast, in Mitrovica & Milne (2003) and Kendall *et al.* (2005) the expression for sea level was based on variations from the following form:

$$SL^O = G - R,$$ (39)

where the superscript 'O' denotes the older theory. In consequence of this definition, the projection of sea level onto the ocean geometry required a modification from the simple form in eq. (4) or (37) to take into account the existence of marine-based ice. Specifically, the projection was written as

$$S^O = SL^O \cdot C^O \cdot \beta,$$ (40)

where

$$C^O = \begin{cases} 1 & \text{if } SL^O > 0 \\ 0 & \text{if } SL^O \le 0, \end{cases}$$ (41)

and

$$\beta = \begin{cases} 1 & \text{where there is no grounded ice} \\ 0 & \text{elsewhere.} \end{cases}$$ (42)

That is, in the old theory, the definition of sea level (39) required a second projection to account for the impact on the ocean geometry of grounded, marine-based ice.

The new theory has two advantages over the old. First, by defining sea level as in eq. (36) or (2), the topography is simply the negative of sea level, as in eq. (3). In contrast, the definition of sea level in eq. (39) is not the negative of topography, at least as defined by data sets such as ETOPO2. Accordingly, in the Mitrovica & Milne (2003) theory, the topography was redefined as ice-corrected topography because sea level and ice-corrected topography would then differ

by sign only. A second advantage of the new theory is that the expression for sea level in eq. (36), since it includes ice height, allows a simpler and more general check for ocean geometry; namely, the ocean height is non-zero anywhere that sea level is positive. This expression is easily generalized when sediments are included as in eqs (2), (4) and (5). In particular, the generalization allows us to avoid a further projection operator that would be zero wherever sediment is thick enough to reach above the ocean surface. Such a projection would be complicated to apply since, as we discussed in the Introduction, sediments, in contrast to the ice load, can be overlain by ocean water.

Thus far, we have focused on the different definitions of sea level adopted in the present formalism relative to the study of Mitrovica & Milne (2003). We end this section by demonstrating that, in the case of no sediment redistribution, the two approaches yield identical results for the change in the ocean thickness.

Using the superscript 'N' for a special scenario with no sediment redistribution, eq. (14) may be written as

$$\Delta S_j = \Delta SL_j^N C_j^N - T_0^N \big[C_j^N - C_0^N \big].$$ (43)

As discussed earlier, the following relations hold between the new and old formalisms: $\Delta SL_j^N = \Delta SL_j^O - \Delta I_j$ and $T_0^N = T_0^O + I_0$. Using these relations in eq. (43), together with the fact that $C^N = C^O \cdot \beta$, yields

$$\Delta S_j = \Delta SL_j^O C_j^O \beta_j - T_0^O \big[C_j^O \beta_j - C_0^O \beta_0 \big]$$
$$- \Delta I_j C_j^O \beta_j - I_0 C_j^O \beta_j + I_0 C_0^O \beta_0.$$ (44)

From eq. (7), the third and fourth terms on the right-hand-side of this expression combine so that

$$\Delta S_j = \Delta SL_j^O C_j^O \beta_j - T_0^O \big[C_j^O \beta_j - C_0^O \beta_0 \big] - I_j C_j^O \beta_j + I_0 C_0^O \beta_0.$$ (45)

From the definition of β in eq. (42), $\beta_i = 0$ wherever I_i is not zero, and thus the third and fourth terms on the right-hand side of eq. (45) vanish. Therefore,

$$\Delta S_j = \Delta SL_j^O C_j^O \beta_j - T_0^O \big[C_j^O \beta_j - C_0^O \beta_0 \big],$$ (46)

which is the sea level equation appearing in Mitrovica & Milne (2003). Thus, when no sediment redistribution is considered, the sea level eq. (14) is formally identical to the expression derived by Mitrovica & Milne (2003).

2.6 Special case of spherically symmetric earth models

The vast majority of studies of postglacial sea level change have adopted spherically symmetric, self-gravitating, Maxwell viscoelastic earth models. In this case, the computation of the total sea level variation, ΔSL [eq. 10, or the two components in the decomposition (23)], may be performed using viscoelastic Love number theory (Peltier 1974). In the Appendix, we briefly outline the theory appropriate to this case, with the inclusion of sediment terms. We consider cases associated with both non-rotating and rotating earth models. In the latter case, sea level is perturbed by the load-induced reorientation of the Earth's rotation vector (e.g. Milne & Mitrovica 1996, 1998). In the former case, this feedback is absent.

All the calculations described in the next section will be based on this special, spherically symmetric theory of sea level change on a rotating Earth. The relevant eqs (see Appendix) are solved up to spherical harmonic degree and order 256. The elastic structure of the earth model is taken from the seismic model PREM (Dziewonski
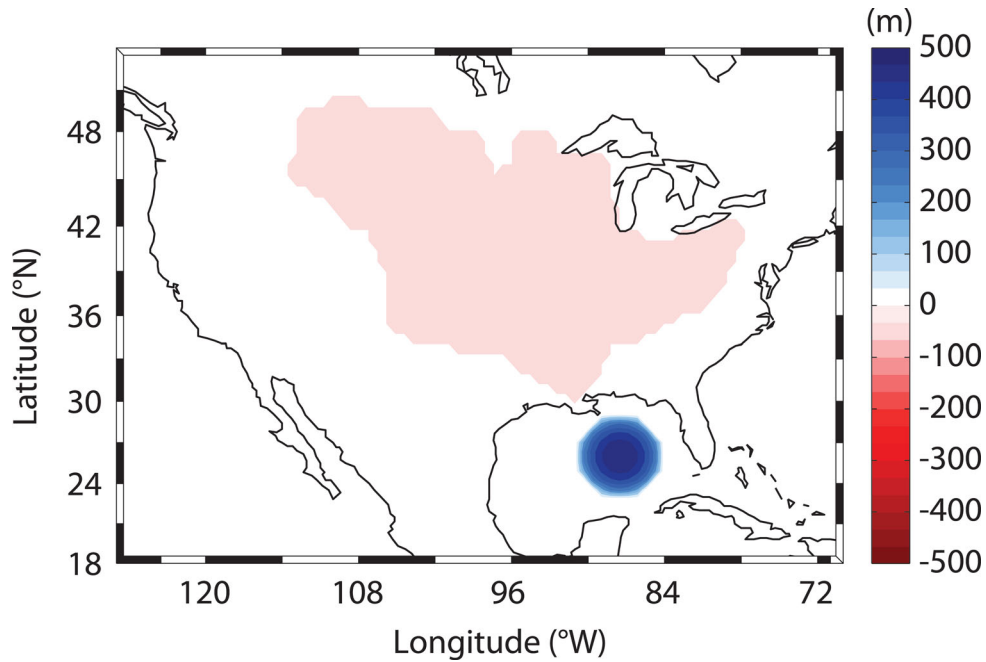
Figure 4. Instantaneous sediment redistribution ΔH adopted in the simplified sediment loading history described in the main text. Erosion over the Mississippi River catchment is assumed to be uniform with thickness equal to 35.9 m, while the axisymmetric deposition at the location of the modern Mississippi fan is circular in horizontal cross-section and parabolic in vertical cross-section. The basal radius of the deposit is 3° and the maximum thickness is 500 m.

& Anderson 1981). Moreover, the radial viscosity profile is the so-called VM2 profile (Peltier 2004). The latter is adopted simply as an illustrative example—none of the conclusions listed below are sensitive to this choice.

3 CASE STUDY: A PULSE OF SEDIMENTATION INTO THE GULF OF MEXICO

As a first case study, we present model results from an idealized scenario in which a large volume of sediment is instantaneously eroded from the Mississippi River catchment and deposited on the Mississippi fan in the Gulf of Mexico (Fig. 4). Our intention here is not to simulate the response of sea level to the full history of sedimentary processes in the Mississippi River system, as this would require estimates of net erosion rates and sediment deposition rates throughout the Mississippi Basin, fan, alluvial plain and delta over the past tens of thousands to hundreds of thousands of years. Instead, our goals are to highlight the physics governing sea level changes associated with sediment redistribution, to isolate the contribution to these changes from perturbations to the height of the sea surface and solid surface, and to assess the accuracy of previous approximations of the gravitationally self-consistent treatment described earlier.

In our idealized scenario for sediment redistribution, the instantaneous erosion of mass from the Mississippi River catchment is assumed to be geographically uniform. The simultaneous deposition of an equal mass of sediment is modelled following Simms *et al.* (2007), with deposition centred at the site of the modern Mississippi fan, in a deposit with a circular basal geometry and an axisymmetric, parabolic vertical cross-section (Fig. 4). That is, the thickness of the sediment deposit, h, as a function of the angular distance from the centre of the deposit, r, is given by

$$h(r) = A \left[1 - \frac{r^2}{r_0^2} \right] \qquad (47)$$

for $r \leq r_0$, where r_0 is the basal radius of the sediment load and A is its maximum thickness. The load is zero for $r > r_0$. In our modelling, we adopted $r_0 = 3°$ and $A = 500$ m, and we centred the deposit at 26°N, 87.5°W. The density of the eroded and deposited sediment was taken to be 2.3 g cm^{-3}. These values for the geometry, location and density of the modelled sedimentary fan were chosen because they are broadly similar to the characteristics of the modern Mississippi fan (Stelting *et al.* 1986; Simms *et al.* 2007). The total mass involved in the redistribution represents roughly half the sediment that was deposited on the Mississippi fan over the last ice age cycle from ~122 ka to the present (Stelting *et al.* 1986). The resulting gravitationally self-consistent sea level response was tracked for a period of 100 kyr following the loading.

It will be instructive, in the discussion below, to compare our predictions of sea level changes in response to the simple scenario of sediment redistribution to the changes predicted for a standard ice age calculation with no sediment redistribution. As an example of the latter, we adopt the gravitationally self-consistent theory described above, with ΔH set to zero. Our calculations adopt the ICE-5G model for the ice history during the last glacial cycle and the VM2 viscosity model (Peltier 2004). In Fig. 5(a), we show predictions of relative sea level (RSL) variations over the last glacial cycle for three sites in and around the Gulf of Mexico (see Fig. 6 for locations). These sites are: (1) the centre of the model sediment deposit; (2) a coastal location in the north (Mobile Bay, Alabama) and (3) a coastal location in the south (San Felipe, Yucatan Peninsula, Mexico). The lower frame of the figure shows the same predictions with the eustatic (i.e. globally uniform) sea level trend associated with the ICE-5G ice history removed.

The RSL trend in the Gulf of Mexico across the last glacial cycle is dominated by the eustatic signal (Fig. 5a), with a general drop in sea level during the glaciation phase, and a more rapid rise in sea level during the deglaciation. However, the gravitational, deformational and rotational signals associated with the ice-ocean mass transfer introduce a site-specific perturbation to this eustatic signal
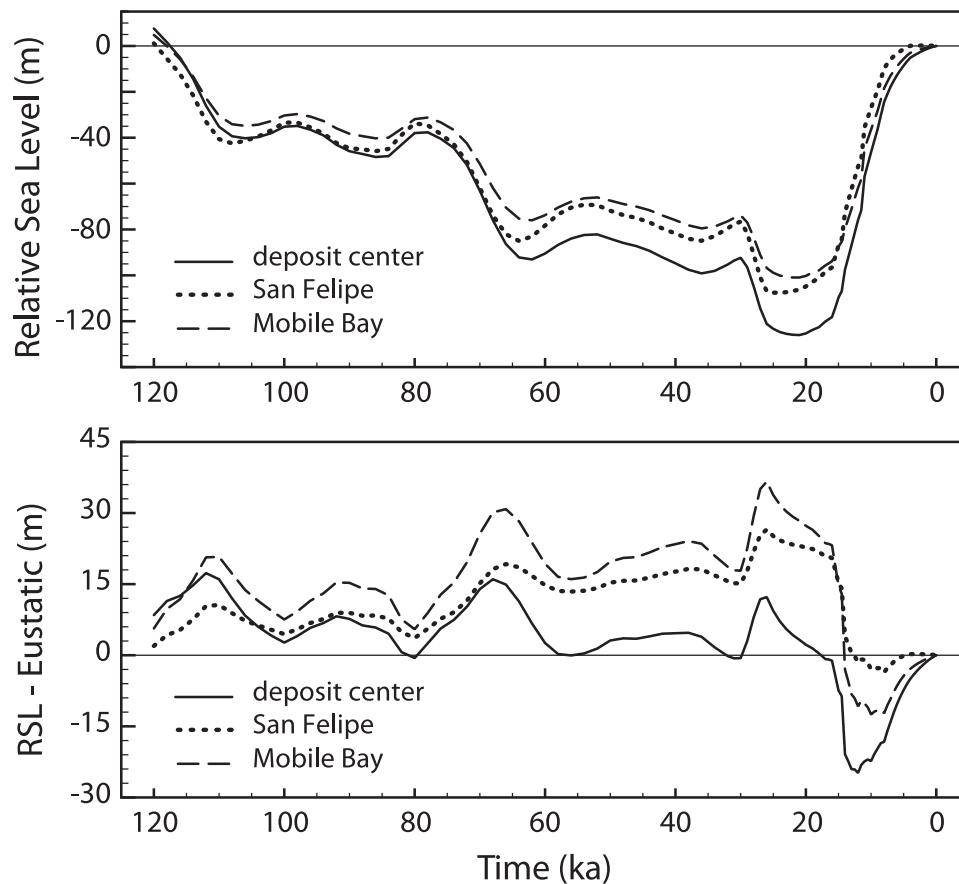
Figure 5. (a) Predictions of relative sea level (RSL) change across the last glacial cycle at the three sites shown in Fig. 6. The predictions are based on the gravitationally self-consistent sea level theory described in the text, with no sediment redistribution applied. The calculations adopt the ICE-5G ice history and the VM2 mantle viscosity model (Peltier 2004) and they are performed using a pseudospectral sea level solver with truncation at spherical harmonic degree and order 256 (Kendall *et al.* 2005). (b) Predictions of RSL at the same three sites considered in frame (a), with the eustatic (i.e. globally uniform component) of the sea level history removed.

which is of order 10–30 m (Fig. 5b). This GIA signal is, given the location of the Gulf of Mexico, a complex superposition of a variety of physical processes associated with ice age sea level changes. These include self-gravitation in the ice-ocean surface mass redistribution, peripheral bulge dynamics, ocean loading effects, continental levering, ocean syphoning and rotational feedback (see Milne & Mitrovica 2008 for a recent review of these processes). It will be useful to compare the amplitude of the sea level signals in Fig. 5(b) with computed perturbations in sea level associated with sediment redistribution.

Fig. 6 shows plots of sea level change after correction for sediment height changes (i.e. $\Delta SL - \Delta H$ in eq. 10) at two times, the instant after the redistribution of the sediments and 100 kyr later. The former, which represents a purely elastic response, has a peak amplitude of ∼20 m, whereas the latter, which reflects the response close to isostatic equilibrium, has a peak amplitude of ∼200 m.

The instantaneous perturbation in sea level due to sediment loading is characterized by a broader zone of sea level rise (and crustal subsidence) than the long-time response of the earth model. This matches the expected behaviour, given that elastic earth models are more efficient than viscous models in filtering out short-wavelength adjustments. In the northwest section of Fig. 6(a), the zone of sea level fall is largely due to crustal uplift associated with the unloading of sediments from the continent. In contrast, the ring of sea level fall encircling the sediment deposit in Fig. 6(b) is due to uplift at

the periphery of the sediment-induced zone of subsidence. That is, the ring reflects the peripheral bulge of the deposit.

The geometry of the response in Fig. 6(b) is such that the predicted sea level rise along the northern coast of the Gulf of Mexico, from ∼84°–92°W, as well as at the northern tip of the Yucatan Peninsula, is ∼20 m. This is comparable to the glacio-isostatic perturbation to sea level (Fig. 5b). The results in Fig. 6 indicate that the magnitude of the sea level signal associated with sediment redistribution from the continent into the Gulf of Mexico, in relation to the ice age signal, depends on the location of the site under consideration and the timescale of the redistribution.

To explore this issue further, we show in Fig. 7 the time history of sea level change due to sediment redistribution at the centre of the sediment redistribution (top row), Mobile Bay, Alabama (middle row) and San Felipe, Mexico (bottom row). The left-side column shows predictions extending over the first 100 kyr, and these results show that isostatic equilibrium has been achieved ∼20 kyr after the pulse of sediment redistribution. The right-side column zooms in on the first 4 kyr of the adjustment. As in Fig. 6, the sea level time-series are corrected for the change in sediment height (i.e. $\Delta SL - \Delta H$ in eq. 10), although this correction is only non-zero within the zones of deposition and erosion. Note that all three sites show a monotonic rise in sea level with time.

The solid red lines and dashed green lines in Fig. 7 are the contributions to the sea level change associated with perturbations in the
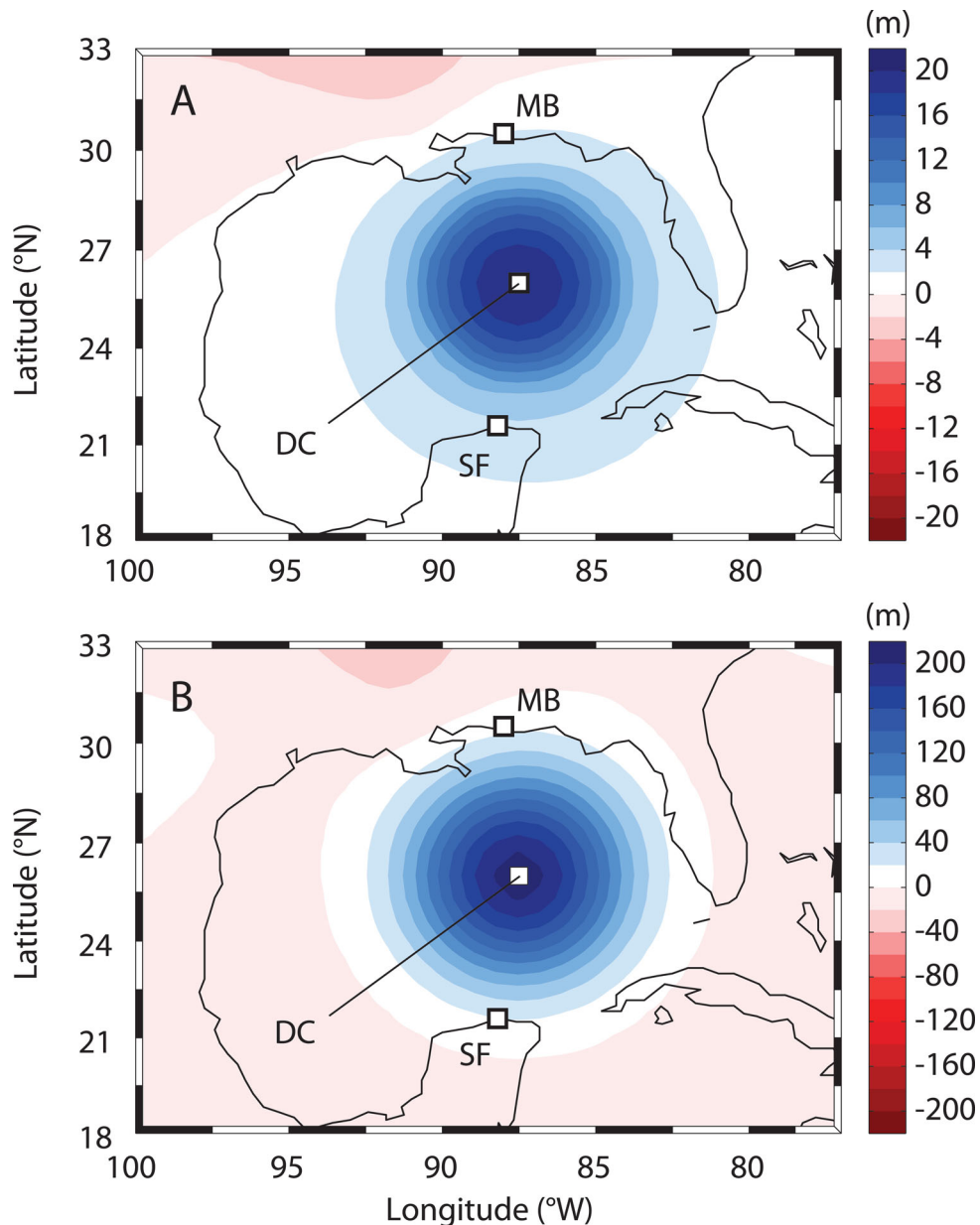
Figure 6. Maps of the total sea level change, not including the change in the height of sediments (i.e. ΔSL from eq. 10 minus ΔH), at two times: (a) the instant after the sediment redistribution is applied; and (b) 100 kyr after the sediment redistribution. The locations of three sites discussed in the text (MB, Mobile Bay; DC, centre of sediment deposit; SF, San Felipe, Mexico) are shown as white squares on the figure.

height of the sea surface ΔG and crust ΔR, respectively. Following eq. (10), ΔG minus ΔR gives the solid blue line in Fig. 7, provided that the height of the sediment ΔH is neglected. At all three sites, the magnitude of the sea-surface equipotential perturbation (red line) is at a maximum just after loading because the redistribution of mass increases the gravitational attraction towards the sediment deposit, and this leads to an instantaneous increase in the sea-surface equipotential within about 2000 km from this location. This is analogous to the so-called 'fingerprint' of sea-surface equipotential change associated with rapid changes in ice mass (e.g. Tamisiea *et al.* 2001). At a given location, the size of the instantaneous perturbation in sea-surface equipotential is a function of position relative to the sediment load. At Mobile Bay, the signals associated with the unloading to the north and loading to the south partially cancel, and the net effect is a relatively small perturbation. In contrast, at San

Felipe, the fingerprint of sediment deposition dominates and the perturbation in sea-surface equipotential is larger. At all locations, the perturbation to sea-surface equipotential diminishes with time as isostatic adjustments act to compensate the direct gravitational effect induced by the sediment redistribution. The signal does not converge to zero because the presence of the elastic lithosphere prevents the system from achieving perfect hydrostatic equilibrium. Finally, within the first few centuries after the sediment redistribution, the radial displacement of the crust dominates the sea level change (i.e. the amplitude of the green dotted line is much larger than the amplitude of the red line in Fig. 7).

The blue lines in Fig. 7 were computed using the same gravitationally self-consistent theory described above for the special case of a spherically symmetric earth model, just as the red and green lines were. We can use these predictions to assess the accuracy of
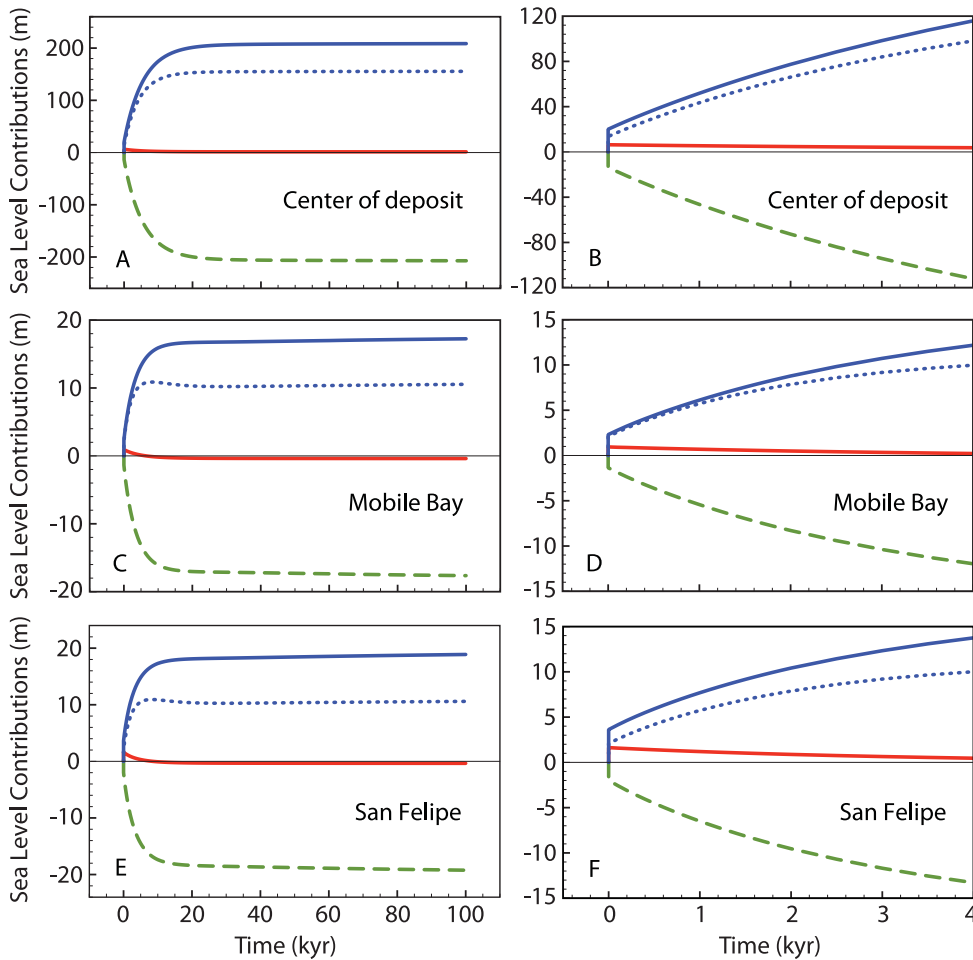
Figure 7. (a) The solid blue line is the predicted sea level change at the centre of the sediment deposit (site 'DC' in Fig. 6), not including the change in the sediment thickness (i.e. ΔSL from eq. 10 with the term ΔH removed), as well as the contributions to this predicted sea level change associated with the change in the height of the sea-surface equipotential ΔG (red line) and the height of the crust ΔR (dashed green line, eq. 10). (b) As in (a) except the plot is limited to the first 4 kyr of the simulation. In both frames, $t = 0$ refers to the time of the model sediment redistribution. The second and third rows are analogous to the first, except they are calculations for the Mobile Bay and Yucatan Peninsula sites (see Fig. 6), respectively. The blue dotted line on all frames is an approximation to the sea level change computed by considering only the radial displacement driven by the sediment load and, in this case, reducing the density of sediments within the Gulf of Mexico to 1.3 g cm^{-3} (see text for a detailed discussion of this approximation).

approximations of the sea level signal associated with sediment re-distribution. For example, we can approximate the sea level change ΔSL_j in eq. (10), after correction for sediment height ΔH_j, and in the absence of ice loads, ΔI_j, as

$$\Delta SL_j - \Delta H_j \sim \Delta G_j^{\dagger} - \Delta R_j^{\dagger}, \qquad (48)$$

where $\Delta G_j^{\dagger}$ and $\Delta R_j^{\dagger}$ are the change in the heights of the sea-surface equipotential and the crust, respectively, driven by the sediment load only, where sediments within the ocean are ascribed a density of $\rho_H - 1$. The latter correction is applied to take into account the reduced (negative) buoyancy of submarine sediments. Since gravitationally self-consistent ocean loading terms are absent on the right-hand side of eq. (48), it is straightforward to solve. If sea-surface equipotential changes are also neglected, then the governing equation becomes

$$\Delta SL_j - \Delta H_j \sim -\Delta R_j^{\dagger}. \qquad (49)$$

The blue dotted lines in each frame of Fig. 7 show results based on the approximation in eq. (49) for the case of our simple pulse of sediment redistribution. In the first $\sim$1 kyr after the redistribution, the error in the prediction for the site at the centre of the deposition

and at San Felipe is approximately equal to the sea-surface equipotential variation neglected in that calculation. The relative error in the approximation (49) at the instant after the sediment redistribution is $\sim$30 and $\sim$45 per cent at these two sites, respectively.

The absolute error progressively increases with time, reaching values of 53.1, 6.7 and 8.3 m (or relative errors of 25, 40 and 45 per cent) after $\sim$20 kyr for the site at the centre of the deposit, Mobile Bay and San Felipe, respectively. This error is almost entirely associated with an underestimation of the crustal displacement, since, by 20 kyr after the deposition, the perturbation to the sea-surface equipotential is very small. The reason for this under-estimation is that the approximation (49) (or the approximation 48) neglects the increase in the water load as the crust subsides in response to the sediment load. As an example, at the centre of the deposit, the gravitationally self-consistent calculation yields a crustal subsidence of $\sim$200 m. Thus, by neglecting the additional $\sim$200 m water load associated with subsidence, one would underestimate crustal subsidence by $\sim$50 m. We note that the error in the approximation (49) at sites along the coastline of the Gulf of Mexico (order $\sim$10 m) is non-negligible relative to the signal in sea level at such sites from GIA (Fig. 5b).

We have computed the sea level change in response to an instantaneous sediment redistribution, and in this case the adjustment timescale for the predictions in Fig. 7 reflects the characteristic viscous adjustment time of the earth model. In the case of the viscosity model we have adopted (VM2), this timescale is of order 10 kyr (Fig. 7). If we had not adopted an instantaneous redistribution of sediment, but nevertheless had considered sediment redistribution that proceeded on a timescale that was rapid relative to the viscous adjustment time, then the predicted sea level response would be comparable to the curves in Fig. 7. If, in contrast, the sediment redistribution was much slower than the viscous adjustment timescale, then the predicted sea level change would mirror the timescale of the forcing. Of course, the sea level response to a sediment redistribution of intermediate timescale would be governed by an interplay between the loading and adjustment timescales. The sea level theory described in this paper accommodates this spectrum of behaviours.

4 FINAL REMARKS

Mitrovica & Milne (2003) extended the sea level equation derived in the classic study of Farrell & Clark (1976) to incorporate shoreline migration due to both local sea level changes and variations in the extent of grounded, marine-based ice. In this study, we further extended the gravitationally self-consistent sea level theory to incorporate the redistribution of sediments. The theory described in the main text provides an exact relationship between changes in the ocean load and changes in global sea level (eq. 14), where the latter includes arbitrary changes in sea surface and crustal heights, as well as ice and sediment geometries (eq. 10). The extension is, as discussed earlier, complicated by the fact that sediments, in contrast to grounded ice, can coexist with water in a given vertical column, and this complexity has required a revision in the treatment of several fields discussed in our previous analyses (Mitrovica & Milne 2003; see Section 2.5). Following earlier work (Kendall *et al.* 2005), we augment the generalized sea level theory with an efficient numerical algorithm that is applicable to earth models of arbitrary complexity (Section 2.4). Moreover, we present special cases of this algorithm, based on viscoelastic Love number theory (Peltier 1974), valid for spherically symmetric (rotating or non-rotating) earth models (Appendix). While we have introduced the new theory in the context of ice age treatments of sea level change, we emphasize that the theory is equally valid for sediment redistribution during non-glacial periods. Because this theory is able to accommodate sediment loads of arbitrary spatial scale and geometry, it is able to quantify the sea level response to small sediment loads as well as to large loads. An application of the formulation to a specific geographic region will provide an assessment of whether the sea level response to a specific sediment loading history is significant relative to other forcings, and thus determine whether sediment loading may be neglected at that site. Because application of the formulation to a given catchment in nature requires estimates of the erosion rate and deposition rate histories across the catchment, uncertainties in the modelled sea level responses will be influenced by the uncertainties in the input erosion rate and deposition rate histories.

As an illustrative case study, we used the spherically symmetric earth model theory described here to compute the sea level perturbation driven by a pulse of sediment redistribution from the North American continent into the Gulf of Mexico. In this regard, we adopted a highly simplified load history that approximates both the spatial scale and amplitude of the sediment deposition. These calculations suggest that the sea level signal due to the sediment redistribution can be equal in magnitude to non-eustatic effects driven by ice age loading at sites along the Gulf Coast, and that both depend on the location of the site and the timescale of the loading. Results from the case study also demonstrate that the relative error incurred by approximating the gravitationally self-consistent sea level change by ignoring the time-varying water load associated with the sediment-induced deformation can reach ∼40 per cent. In a companion paper, we will present predictions of sea level changes based on more realistic space–time models of continental erosion and sediment deposition in the Gulf of Mexico.

REFERENCES

Clark, J.A., Farrell, W.E. & Peltier, W.R., 1978. Global changes in postglacial sea level: a numerical calculation, *Quat. Res.,* **9,** 265–287.

Davis, J.E., Latychev, K., Mitrovica, J.X., Kendall, R. & Tamisiea, M.E., 2008. Glacial isostatic adjustment in 3-D Earth models: implications for tide gauge analyses along the U.S. east coast, *J. Geodyn.,* **46,** 90–94.

Dziewonski, A.M. & Anderson, D.L., 1981. Preliminary reference Earth model (PREM), *Phys. Earth planet. Inter.,* **25,** 297–356.

Farrell, W.E. & Clark, J.A., 1976. On postglacial sea level, *Geophys. J. R. astr. Soc.,* **46,** 647–667.

Johnston, P., 1993. The effect of spatially non-uniform water loads on predictions of sea level change, *Geophys. J. Int.,* **114,** 615–634.

Kendall, R.A, Mitrovica, J.X. & Milne, G.A., 2005. On post-glacial sea level: II. Numerical formulation and comparative results on spherically symmetric models, *Geophys. J. Int.,* **161,** 679–706.

Kendall, R.A, Latychev, K., Mitrovica, J.X., Davis, J.E. & Tamisiea, M.E., 2006. Decontaminating tide gauge records for the contaminating influence of glacial isostatic adjustment: the potential impact of 3-D Earth structure, *Geophys. Res. Lett.,* **33,** L24318, doi:10.1029/2006GL028448.

Lambeck, K., Purcell, A., Johnston, P., Nakada, M. & Yokoyama, Y., 2003. Water-load definition in the glacio-hydro-isostatic sea-level equation, *Quat. Sci. Rev.,* **21,** 309–318.

Latychev, K., Mitrovica, J.X., Tromp, J., Tamisiea, M.E., Komatitsch, D. & Christara, C.C., 2005. Glacial isostatic adjustment on 3-D Earth models: a finite volume formulation, *Geophys. J. Int.,* **161,** 421–444.

Martinec, Z., 2000. Spectral–finite element approach to three-dimensional viscoelastic relaxation in a spherical earth, *Geophys. J. Int.,* **142,** 117–141.

Milne, G.A., 1998. Refining models of the glacial isostatic adjustment process, *PhD thesis,* University of Toronto, Toronto.

Milne, G.A. & Mitrovica, J.X., 1996. Postglacial sea-level change on a rotating Earth: first results from a gravitationally self-consistent sea-level equation, *Geophys. J. Int.,* **126,** F13–F20.

Milne, G.A. & Mitrovica, J.X., 1998. Postglacial sea-level change on a rotating Earth, *Geophys. J. Int.,* **133,** 1–10.

Milne, G.A. & Mitrovica, J.X., 2008. Searching for eustasy in deglacial sea-level histories, *Quat. Sci. Rev.,* **27,** 2292–2302.

Milne, G.A., Mitrovica, J.X. & Davis, J.L., 1999. Near-field hydro-isostasy: the implementation of a revised sea-level equation, *Geophys. J. Int.,* **139,** 464–482.

Mitrovica, J.X., 2003. Recent controversies in predicting post-glacial sea-level change, *Quat. Sci. Rev.,* **22,** 127–133.

Mitrovica, J.X. & Milne, G.A., 2003. On post-glacial sea level: I. General theory, *Geophys. J. Int.,* **154,** 253–267.

Mitrovica, J.X. & Peltier, W.R., 1989. Pleistocene deglaciation and the global gravity field, *J. geophys. Res.,* **94,** 13 651–13 671.

Mitrovica, J.X. & Peltier, W.R., 1991. On post-glacial geoid subsidence over the equatorial oceans, *J. geophys. Res.,* **96,** 20 053–20 071.

Paulson, A., Zhong, S. & Wahr, J., 2005. Modelling post-glacial rebound with lateral viscosity variations, *Geophys. J. Int.,* **163,** 357–371.

Peltier, W.R., 1974. The impulse response of a Maxwell Earth, *Rev. Geophys.,* **12,** 649–669.

Peltier, W.R., 1994. Ice age paleotopography, *Science,* **265,** 195–201.

Peltier, W.R., 1998. 'Implicit ice' in the global theory of glacial isostatic adjustment, *Geophys, Res. Lett.,* **25,** 3955–3958.

Peltier, W.R., 2004. Global glacial isostasy and the surface of the ice-age Earth: the ICE-5G (VM2) model and GRACE, *Ann. Rev. Earth planet. Sci.,* **32,** 111–149.

Peltier, W.R. & Andrews, J.T., 1976. Glacial isostatic adjustment I: the forward problem, *Geophys. J. R. astr. Soc.,* **46,** 605–646.

Peltier, W.R., Farrell, W.E. & Clark, J.T., 1978. Glacial isostasy and relative sea level: a global finite element model, *Tectonophys.,* **50,** 81–110.

Simms, A.R., Lambeck, K., Purcell, A., Anderson, J.B. & Rodriguez, A.B., 2007. Sea-level history of the Gulf of Mexico since the Last Glacial Maximum with implications for the melting history of the Laurentide Ice Sheet, *Quat. Sci. Rev.,* **26,** 920–940.

Stelting, C.E. *et al.*, 1986. Late Pleistocene seismic stratigraphy of the Mississippi Fan, in *Initial Reports of the Deep Sea Drilling Project,* Vol. 96, pp. 437–456, eds Bouma, A.H. *et al.*, U.S. Govt. Printing Office, Washington.

Tamisiea, M.E., Mitrovica, J.X., Milne, G.A. & Davis, J.L., 2001. Global geoid and sea level changes due to present-day ice mass fluctuations, *J. geophys. Res.,* **106,** 30 849–30 863.

Tromp, J. & Mitrovica, J. X., 1999. Surface loading of a viscoelastic Earth— I. General theory, *Geophys. J. Int.,* **137,** 847–855.

Tushingham, A.M. & Peltier, W.R., 1991. ICE-3G: a new global model of late Pleistocene deglaciation based upon geophysical predictions of postglacial relative sea level, *J. geophys. Res.,* **96,** 4497–4523.

United States Department of Commerce National Oceanic and Atmospheric Administration National Geophysical Data Center, 2001. 2-minute Gridded Global Relief Data (ETOPO2). Available at: http://www.ngdc.noaa.gov/mgg/fliers/01mgg04.html, accessed 2006.

Wu, P. & Peltier, W.R., 1983. Glacial isostatic adjustment and the free air gravity anomaly as a constraint on deep mantle viscosity, *Geophys. J. R. astr. Soc.,* **74,** 377–449.

Wu, P. & Peltier, W.R., 1984. Pleistocene deglaciation and the Earth's rotation: a new analysis, *Geophys. J. R. astr. Soc.,* **76,** 753–792.

Wu, P. & van der Wal, W., 2003. Postglacial sea levels on a spherical, self-gravitating viscoelastic Earth: effects of lateral viscosity variations in the upper mantle on the inference of viscosity contrasts in the lower mantle, *Earth planet. Sci. Lett.,* **211,** 57–68.

Zhong, S., Paulson, A. & Wahr, J., 2003. Three-dimensional finite element modeling of Earth's viscoelastic deformation: effects of lateral variations in lithospheric thickness, *Geophys. J. Int.,* **155,** 679–695.

APPENDIX A: EXPRESSIONS FOR ΔSL IN THE CASE OF SPHERICALLY SYMMETRIC EARTH MODELS

In this appendix, we derive expressions for the change in sea level, ΔSL, for the case of spherically symmetric (i.e. depth-varying) Maxwell viscoelastic earth models by making use of viscoelastic Love number theory (Peltier 1974). This section and the next extend the treatment described in Kendall *et al.* (2005) to include terms associated with sediment redistribution. We begin with the case of non-rotating earth models.

A1 Non-rotating earth models

For spherically symmetric earth models, any scalar geophysical signal of interest may be written as a convolution of the appropriate Green's function with the surface mass load. If we denote a generalized scalar quantity as $\Delta \chi$, we may write

$$\Delta \chi = \int_{-\infty}^{t} \iint_{\Omega} \Delta L(\theta', \psi', t') \cdot GF(\gamma, t - t') \, d\Omega' \, dt', \quad (A1)$$

where GF denotes the Green's function, and θ and ψ represent the colatitude and east longitude, respectively. The parameter γ is the angle between the observation point, (θ, ψ), and the load point, (θ', ψ'), and it is given by

$$\cos \gamma = \cos \theta \cos \theta' + \sin \theta \sin \theta' \cos (\psi - \psi'). \quad (A2)$$

A computation of the spatially varying component of the sea level change, $\Delta \mathcal{SL}$ (eq. 24), requires expressions for $\Delta \mathcal{G}$ and ΔR. Using the form (A1), we may write

$$\Delta \mathcal{G} = \int_{-\infty}^{t} \iint_{\Omega} \Delta L(\theta', \psi', t') \frac{\phi(\gamma, t - t')}{g} \, d\Omega' \, dt', \quad (A3)$$

$$\Delta R = \int_{-\infty}^{t} \iint_{\Omega} \Delta L(\theta', \psi', t') \Gamma(\gamma, t - t') \, d\Omega' \, dt', \quad (A4)$$

where $\phi(\gamma, t)$ and $\Gamma(\gamma, t)$ are Green's functions for the gravitational potential perturbation and radial displacement of the solid surface, respectively. Combining eqs (24), (A3) and (A4) gives

$$\Delta \mathcal{SL}_j = \int_{-\infty}^{t_j} \iint_{\Omega} \Delta L(\theta', \psi', t')$$
$$\times \left[\frac{\phi(\gamma, t_j - t')}{g} - \Gamma(\gamma, t_j - t') \right] d\Omega' \, dt' - \Delta H_j - \Delta I_j. \quad (A5)$$

In the time-domain, the viscoelastic k and h Love numbers at spherical harmonic degree ℓ may be written in the normal mode form (Peltier 1974; Tromp & Mitrovica 1999)

$$k_\ell(t) = k_\ell^E \delta(t) + \sum_{k=1}^{K} r_k'^\ell e^{-s_k^\ell t}, \quad (A6)$$

$$h_\ell(t) = h_\ell^E \delta(t) + \sum_{k=1}^{K} r_k^\ell e^{-s_k^\ell t}, \quad (A7)$$

where each equation is comprised of an instantaneous elastic response (which includes a Dirac-delta function time dependence) and a non-elastic response represented as a sum of K modes of pure exponential decay. The viscoelastic structure of the earth model is embedded within these Love numbers and the parameters defining them may be combined to construct the Green's functions required in eq. (A5) (Mitrovica & Peltier 1989):

$$\phi(\gamma, t) = \frac{ag}{M_e} \sum_{\ell=0}^{\infty} \left[\delta(t) + k_\ell^E \delta(t) + \sum_{k=1}^{K} r_k'^\ell e^{-s_k^\ell t} \right] P_\ell(\cos \gamma), \quad (A8)$$

$$\Gamma(\gamma, t) = \frac{a}{M_e} \sum_{\ell=0}^{\infty} \left[h_\ell^E \delta(t) + \sum_{k=1}^{K} r_k^\ell e^{-s_k^\ell t} \right] P_\ell(\cos \gamma), \quad (A9)$$

where a and M_e are the radius and mass of the Earth and P_ℓ is the Legendre polynomial at degree ℓ.

If we model the total surface mass load variation ΔL (eq. 17) at time t as a series of Heaviside step increments

$$\Delta L = \sum_{n=0}^{N} [\rho_{\mathrm{w}} \delta S_n + \rho_{\mathrm{I}} \delta I_n + \rho_{\mathrm{H}} \delta H_n] \mathcal{H}(t - t_n), \tag{A10}$$

where

$$\mathcal{H}(t - t_n) = \begin{cases} 0 & \text{if } t < t_n \\ 1 & \text{if } t \geq t_n, \end{cases} \tag{A11}$$

then the time convolutions in eq. (A5) can be performed analytically to yield

$$\begin{aligned}
\Delta \mathcal{SL}_j &= \frac{a}{M_{\mathrm{e}}} \sum_{\ell=0}^{\infty} E_{\ell} \iint_{\Omega} \big[\rho_{\mathrm{w}} \Delta S_j(\theta', \psi') + \rho_{\mathrm{I}} \Delta I_j(\theta', \psi') \\
&\quad + \rho_{\mathrm{H}} \Delta H_j(\theta', \psi') \big] P_{\ell}(\cos \gamma) \, d\Omega' \\
&\quad + \frac{a}{M_{\mathrm{e}}} \sum_{\ell=0}^{\infty} \sum_{n=0}^{N} \mathcal{H}(t_j - t_n) \beta(\ell, t_n, t_j) \\
&\quad \times \iint_{\Omega} \big[\rho_{\mathrm{w}} \delta S_n(\theta', \psi') + \rho_{\mathrm{I}} \delta I_n(\theta', \psi') \\
&\quad + \rho_{\mathrm{H}} \delta H_n(\theta', \psi') \big] P_{\ell}(\cos \gamma) \, d\Omega' - \Delta H_j - \Delta I_j,
\end{aligned} \tag{A12}$$

where

$$E_{\ell} = 1 + k_{\ell}^{E} - h_{\ell}^{E} \tag{A13}$$

and

$$\beta(\ell, t_n, t_j) = \sum_{k=1}^{K} \frac{r_k'^{\ell} - r_k^{\ell}}{s_k^{\ell}} \big[1 - e^{-s_k^{\ell}(t_j - t_n)} \big]. \tag{A14}$$

To complete the derivation we seek an analytic approach to the 2-D spatial convolutions in eq. (A12). To this end, let us introduce a general spherical harmonic decomposition of a scalar field χ.

$$\chi(\theta, \psi) = \sum_{\ell=0}^{\infty} \sum_{m=-\ell}^{\ell} \chi_{\ell m} Y_{\ell m}(\theta, \psi), \tag{A15}$$

and the $Y_{\ell m}$ are associated spherical harmonics normalized such that

$$\iint_{\mathrm{sphere}} Y_{\ell' m'}(\theta, \psi) Y_{\ell m}^{*}(\theta, \psi) \sin \theta \, d\theta \, d\psi = 4\pi \delta_{\ell' \ell} \delta_{m'm}, \tag{A16}$$

where the asterisk denotes the complex conjugate, and δ is the Dirac-delta function. In this case, one can show that (Mitrovica & Peltier 1991)

$$\iint_{\Omega} \chi(\theta', \psi') P_{\ell}(\cos \gamma) \, d\Omega' = \frac{4\pi a^2}{2\ell + 1} \sum_{m=-\ell}^{\ell} \chi_{\ell m} Y_{\ell m}(\theta, \psi). \tag{A17}$$

Applying (A15) and (A17) to (A12) yields the expression

$$\begin{aligned}
\Delta \mathcal{SL}_j &= \sum_{\ell, m} T_{\ell} E_{\ell} \big[\rho_{\mathrm{I}} \Delta I_{\ell m, j} + \rho_{\mathrm{w}} \Delta S_{\ell m, j} + \rho_{\mathrm{H}} \Delta H_{\ell m, j} \big] Y_{\ell m}(\theta, \psi) \\
&\quad + \sum_{\ell, m} T_{\ell} \sum_{n=0}^{j-1} \beta(\ell, t_n, t_j) \big[\rho_{\mathrm{w}} \delta S_{\ell m, n} + \rho_{\mathrm{I}} \delta I_{\ell m, n} + \rho_{\mathrm{H}} \delta H_{\ell m, n} \big] Y_{\ell m}(\theta, \psi) \\
&\quad - \sum_{\ell, m} \Delta H_{\ell m, j} Y_{\ell m}(\theta, \psi) - \sum_{\ell, m} \Delta I_{\ell m, j} Y_{\ell m}(\theta, \psi),
\end{aligned} \tag{A18}$$

where

$$T_{\ell} = \frac{4\pi a^3}{(2\ell + 1) M_{\mathrm{e}}} \tag{A19}$$

and we have used the short form

$$\sum_{\ell m} \equiv \sum_{\ell=0}^{\infty} \sum_{m=-\ell}^{\ell} . \tag{A20}$$

We have also introduced subscripts of the form $\chi_{\ell m, j}$ and $\chi_{\ell m, n}$ to indicate spherical harmonic coefficients $\chi_{\ell m}$ at time steps t_j and t_n, respectively.

Using eq. (A18) in the conservation formula (28) yields an expression for the spatially invariant term in the total sea level variation $\Delta \Phi_j$.

$$\frac{\Delta \Phi_j}{g} = \frac{1}{C_{00, j}} \left(-\frac{\rho_{\mathrm{I}}}{\rho_{\mathrm{w}}} \Delta I_{00, j} - RO_{00, j} + TO_{00, 0} \right), \tag{A21}$$

where we have used the projections

$$\begin{aligned}
RO_j &= \Delta \mathcal{SL}_j C_j \\
&= \sum_{\ell, m} RO_{\ell m, j} Y_{\ell m}(\theta, \psi)
\end{aligned} \tag{A22}$$

and

$$\begin{aligned}
TO_j &= T_0 \big[C_j - C_0 \big] \\
&= \sum_{\ell, m} TO_{\ell m, j} Y_{\ell m}(\theta, \psi).
\end{aligned} \tag{A23}$$

Finally, we rewrite (A18) and (A21) to include algorithm counters i and k, as in the main text. First, the spectral components of $\Delta \mathcal{SL}$ in eq. (A18) are

$$\begin{aligned}
\big[\Delta \mathcal{SL}_{\ell m, j} \big]^{i-1, k} &= T_{\ell} E_{\ell} \big(\rho_{\mathrm{I}} \big[\Delta I_{\ell m, j} \big]^{k-1} + \rho_{\mathrm{w}} \big[\Delta S_{\ell m, j-1} \big]^{i=\infty, k} \\
&\quad + \rho_{\mathrm{w}} \big[\delta S_{\ell m, j} \big]^{i-1, k} + \rho_{\mathrm{H}} \Delta H_{\ell m, j} \big) \\
&\quad + T_{\ell} \sum_{n=0}^{j-1} \beta(\ell, t_n, t_j) \big(\rho_{\mathrm{w}} \big[\delta S_{\ell m, n} \big]^{i=\infty, k} \\
&\quad + \rho_{\mathrm{I}} \big[\delta I_{\ell m, n} \big]^{k-1} + \rho_{\mathrm{H}} \delta H_{\ell m, n} \big) - \Delta H_{\ell m, n} \\
&\quad - \big[\Delta I_{\ell m, n} \big]^{k-1},
\end{aligned} \tag{A24}$$

and similarly, eq. (A21) becomes

$$\begin{aligned}
\left[\frac{\Delta \Phi_j}{g} \right]^{i-1, k} &= \frac{1}{\big[C_{00, j} \big]^{k-1}} \left\{ -\frac{\rho_{\mathrm{I}}}{\rho_{\mathrm{w}}} \big[\Delta I_{00, j} \big]^{k-1} \right. \\
&\quad \left. - \big[RO_{00, j} \big]^{i-1, k} + \big[TO_{00, j} \big]^{k-1} \right\},
\end{aligned} \tag{A25}$$

where

$$\begin{aligned}
RO_j^{i-1, k} &= \Delta \mathcal{SL}_j^{i-1, k} C_j^{k-1} \\
&= \sum_{\ell, m} \big[RO_{\ell m, j} \big]^{i-1, k} Y_{\ell m}(\theta, \psi)
\end{aligned} \tag{A26}$$

and

$$\begin{aligned}
TO_j^{k-1}(\theta, \psi) &= T_0^{k-1} \big[C_j^{k-1} - C_0^{k-1} \big] \\
&= \sum_{\ell, m} \big[TO_{\ell m, j} \big]^{k-1} Y_{\ell m}(\theta, \psi).
\end{aligned} \tag{A27}$$

These equations are used in (30), where all other operations are performed in the spatial domain.

A2 Rotating earth models

Next, we extend the expressions derived above to include the impact on sea level of perturbations in the Earth's rotation vector. An accurate normal mode treatment of ice age Earth rotation has been derived by Mitrovica *et al.* (2005), following earlier work by Wu & Peltier (1984). Their theory yields, for an arbitrary surface mass load (in our case, a superposition of ice, water and sediment redistributions), a time-varying rotation vector. This time-series can be converted to an evolving centrifugal potential, which we will denote by $\Lambda(\theta, \psi, t)$. If we decompose the centrifugal potential into its value prior to the onset of loading and a perturbation from this value, then, following the notation in eq. (7) we can write

$$\Lambda(\theta, \psi, t) = \Lambda(\theta, \psi, t_0) + \Delta\Lambda(\theta, \psi, t). \tag{A28}$$

The second term on the right-hand side of this equation is the so-called 'rotational driving potential'. The driving potential is non-zero only at degree zero and two, and thus the spherical harmonic decomposition of this term is

$$\Delta\Lambda(\theta, \psi, t_j) = \Delta\Lambda_{00,j} Y_{00}(\theta, \psi) + \sum_{m=-2}^{2} \Delta\Lambda_{2m,j} Y_{2m}(\theta, \psi). \tag{A29}$$

Analytic expressions relating these harmonic components to the perturbation in the rotation vector are given in Milne & Mitrovica (1998).

The Earth's response to the driving potential is governed by the so-called viscoelastic tidal (or tidal-effective) Love numbers which, in analogy with eqs (A6) and (A7), have the form (Peltier 1974):

$$k_\ell^T(t) = k_\ell^{T,E}\delta(t) + \sum_{k=1}^{K} r_k^{\prime\ell,T} e^{-s_k^\ell t}, \tag{A30}$$

$$h_\ell^T(t) = h_\ell^{T,E}\delta(t) + \sum_{k=1}^{K} r_k^{\ell,T} e^{-s_k^\ell t}. \tag{A31}$$

Note that the tidal Love numbers have the same inverse decay times as the load Love numbers, but they have distinct modal amplitudes.

Using eqs (A28)–(A31), one can extend eq. (A18) to include the sea level response to the rotational driving potential (Kendall *et al.* 2005). Specifically

$$\Delta\mathcal{SL}_j$$

$$= \sum_{\ell,m} T_\ell E_\ell \big[\rho_{\mathrm{I}} \Delta I_{\ell m,j} + \rho_{\mathrm{W}} \Delta S_{\ell m,j} + \rho_{\mathrm{H}} \Delta H_{\ell m,j}\big] Y_{\ell m}(\theta, \psi)$$

$$+ \sum_{\ell,m} T_\ell \sum_{n=0}^{j-1} \beta(\ell, t_n, t_j)\big[\rho_{\mathrm{W}}\delta S_{\ell m,n}+\rho_{\mathrm{I}}\delta I_{\ell m,n}+\rho_{\mathrm{H}}\delta H_{\ell m,n}\big] Y_{\ell m}(\theta, \psi)$$

$$+ \frac{1}{g} \sum_{\ell,m} E_\ell^T \Delta\Lambda_{\ell m,j} + \frac{1}{g} \sum_{\ell,m} \sum_{n=0}^{j-1} \beta^T(\ell, t_n, t_j)\delta\Lambda_{\ell m,n}$$

$$- \sum_{\ell,m} \Delta H_{\ell m,j} Y_{\ell m}(\theta, \psi)$$

$$- \sum_{\ell,m} \Delta I_{\ell m,j} Y_{\ell m}(\theta, \psi), \tag{A32}$$

where

$$E_\ell^T = 1 + k_\ell^{T,E} - h_\ell^{T,E} \tag{A33}$$

and

$$\beta^T(\ell, t_n, t_j) = \sum_{k=1}^{K} \frac{r_k^{\prime\ell,T} - r_k^{\ell,T}}{s_k^\ell}\big[1 - e^{-s_k^\ell(t_j-t_n)}\big]. \tag{A34}$$

In a calculation of the total perturbation in global sea level, eq. (A32) is augmented by the expression for the globally uniform shift given by eq. (28).

Using eq. (A32), the algorithm defined by eq. (A24) can be extended to include rotational effects

$$[\Delta\mathcal{SL}_{\ell m,j}]^{i-1,k} = T_\ell E_\ell\big(\rho_{\mathrm{I}}\big[\Delta I_{\ell m,j}\big]^{k-1} + \rho_{\mathrm{W}}\big[\Delta S_{\ell m,j-1}\big]^{i=\infty,k}$$

$$+ \rho_{\mathrm{W}}\big[\delta S_{\ell m,j}\big]^{i-1,k} + \rho_{\mathrm{H}}\Delta H_{\ell m,j}\big)$$

$$+ T_\ell \sum_{n=0}^{j-1} \beta(\ell, t_n, t_j)\big(\rho_{\mathrm{W}}\big[\delta S_{\ell m,n}\big]^{i=\infty,k}$$

$$+ \rho_{\mathrm{I}}\big[\delta I_{\ell m,n}\big]^{k-1} + \rho_{\mathrm{H}}\delta H_{\ell m,n}\big)$$

$$+ \frac{1}{g} E_\ell^T \big(\big[\Delta\Lambda_{\ell m,j-1}\big]^{i=\infty,k} + \big[\delta\Lambda_{\ell m,j}\big]^{i-1,k}\big)$$

$$+ \frac{1}{g} \sum_{n=0}^{j-1} \beta^T(\ell, t_n, t_j)\big[\delta\Lambda_{\ell m,n}\big]^{i=\infty,k}$$

$$- \Delta H_{\ell m,n} - \big[\Delta I_{\ell m,n}\big]^{k-1}. \tag{A35}$$

In this case, the spatially invariant contribution to the total global sea level perturbation is given by eq. (A25).